npj | quantum materials

Article

Published in partnership with Nanjing University

https://doi.org/10.1038/s41535-024-00663-1

Unveiling the quasiparticle behaviour in the pressure-induced high-T_c phase of an iron-chalcogenide superconductor

Z. Zajicek[1,6], **P. Reiss**[1,2,6], **D. Graf**[3], **J. C. A. Prentice**[4], **Y. Sadki**[1], **A. A. Haghighirad**[1,5] &
A. I. Coldea[1]

Superconductivity of iron chalocogenides is strongly enhanced under applied pressure yet its underlying pairing mechanism remains elusive. Here, we present a quantum oscillations study up to 45 T in the high-T_c phase of tetragonal $FeSe_{0.82}S_{0.18}$ up to 22 kbar. Under applied pressure, the quasi-two-dimensional multi-band Fermi surface expands and the effective masses remain large, whereas the superconductivity displays a threefold enhancement. Comparing with chemical pressure tuning of $FeSe_{1-x}S_x$, the Fermi surface expands in a similar manner but the effective masses and T_c are suppressed. These differences may be attributed to the changes in the density of states influenced by the chalcogen height, which could promote stronger spin fluctuations pairing under pressure. Furthermore, our study also reveals unusual scattering and broadening of superconducting transitions in the high-pressure phase, indicating the presence of a complex pairing mechanism.

One direct route to enhance conventional superconductivity towards room temperature is to apply extreme pressures to light elements to strengthen the electron–phonon coupling[1]. In the case of iron-based superconductors, applying pressure to bulk FeSe leads to a fourfold enhancement in superconductivity towards 37 K under ~40 kbar[2–4]. Due to the small Fermi surface of FeSe, various competing electronic nematic, magnetic and superconducting orders can emerge on similar energy scales which could be stabilized in different pressure regimes[5]. At low pressures, FeSe has a small Fermi energy and exhibits a nematic electronic phase driven by orbital degrees of freedom and strong electronic correlations, leading to highly anisotropic electronic and superconducting behaviour[6–8]. On the other hand, an increase in the Fermi energy may favour the stability of a magnetic phase[5]. Experimentally, both superconducting and magnetic phases could coexist under pressure[9], along with additional structural effects[10] posing challenges in understanding the high-T_c high-pressure phase.

In a similar manner to applied pressure, chemical pressure induced by the isovalent substitution of selenium for sulphur can suppress nematicity[11]. Surprisingly, within the tetragonal phase the superconductivity is not enhanced, no magnetic order is detected, and electronic correlations are significantly weakened[11–14]. Across the nematic end point of $FeSe_{1-x}S_x$, changes in the superconducting gap structure[15,16], and a topological transition into an ultranodal phase with Bogoliubov Fermi surface phases has been proposed[17]. Notably, by combining both applied and chemical pressure, the anomalies associated with the magnetic order are shifted to higher pressures with increased sulphur substitution in $FeSe_{1-x}S_x$[18]. This decoupling of overlapping nematic and magnetic phases allows for a deeper understanding of their individual contribution to superconductivity and provides an opportunity to explore the region of a quantum nematic phase transition[14,19–21]. Despite the robustness of the high-T_c phase under applied pressure, the presence of the magnetic order is highly sensitive to the isoelectronic substitution, disorder, and uniaxial effects[18,22–24]. This raises the fundamental question whether the magnetically mediated pairing is responsible for superconductivity, which needs to be clarified by having direct access to the Fermi surface topology and electronic correlations in the high-pressure phase.

Quantum oscillations provide a direct measurement of Fermi surfaces and the properties of quasiparticles involved in the superconducting pairing mechanism. Unlike other spectroscopic techniques like ARPES and STM, which probe the electronic structure, quantum oscillations offer access to the high-T_c high-pressure phase of $FeSe_{1-x}S_x$. Quantum oscillations have been observed at ambient pressure in FeSe[25–27] and $FeSe_{1-x}S_x$[7,28], revealing multiple Fermi surface pockets and relatively large effective masses which are strongly suppressed by chemical pressure[12]. Fermi surfaces expand via chemical pressure towards FeS and a Lifshitz transition has been identified

---

[1]Clarendon Laboratory, Department of Physics, University of Oxford, Oxford, UK. [2]Max Planck Institute for Solid State Research, Stuttgart, Germany. [3]National High Magnetic Field Laboratory and Department of Physics, Florida State University, Tallahassee, FL, USA. [4]Department of Materials, University of Oxford, Oxford, UK. [5]Institute for Quantum Materials and Technologies, Karlsruhe Institute of Technology, Karlsruhe, Germany. [6]These authors contributed equally: Z. Zajicek, P. Reiss. e-mail: amalia.coldea@physics.ox.ac.uk

at the boundary of the nematic phase[7,19,28]. In contrast, quantum oscillations in FeSe under high pressure primarily detect low frequencies, suggesting a Fermi surface reconstruction in the presence of the magnetic order[29]. These observations highlight the importance of understanding Fermi surfaces and quasiparticles in different regimes to identify the relevant features for superconductivity.

In this study, we experimentally investigate the electronic behaviour of the tetragonal high-T_c phase of $FeSe_{0.82}S_{0.18}$ under high magnetic fields up to 45 T and applied pressures up to 22 kbar. The observed quantum oscillations probe directly the evolution of the Fermi surfaces and the quasiparticle behaviour with increasing pressure. Our results reveal the expansion of the Fermi surface and large and weakly varying cyclotron effective masses, in particular for the outer hole pockets. In comparison, the superconducting critical temperature displays a gentle decrease at low pressures (around 7 K at ~11 kbar), followed by a significant threefold increase (~19 K at ~21 kbar). In addition, the high-pressure phase harbours broad superconducting transition widths and larger residual resistivity and we detect unusual disparity between the small and large-angle scattering. These findings reveal a complex normal behaviour and suggest the involvement of additional pairing channels to stabilize the high-T_c phase under pressure.

Results

Temperature dependence of resistivity with applied pressure

Figure 1a shows the temperature dependence of the longitudinal resistivity, ρ_{xx}, of a tetragonal sample S1 under various applied pressures. At ambient pressure, sample S1 displays a sharp superconducting transition. In contrast, sample S2 from the same batch displays an additional weak anomaly at $T_s \sim 26$ K, which is quickly suppressed at low pressures (~1 kbar) (see the first derivative in Supplementary Fig. 1)[12]. Different samples have similar values of $T_c \sim 7(1)$ K in the tetragonal phase, which remains relatively unchanged up to 11 kbar, as shown in Fig. 1c. Interestingly, at high pressures the superconductivity is enhanced by up to a factor of 3 towards 19 K at 21 kbar for sample S1 (see also Supplementary Figs. 5 and 7). Furthermore, the width of the superconducting transition broadens at higher pressures, both in temperature and magnetic field, despite the absence of any competing phases in this regime (see Fig. 1a, b and Supplementary Figs. 5b and 12). Notably, comparable $T_c \sim 20$ K is also detected in FeSe under a similar applied pressure, but in the vicinity of the magnetic phase[29], as well as in $Cu_xFe_{1-x}Se$, in which the signatures of magnetism are washed away by impurity scattering[23]. Normally, the applied pressure is expected to increase the bandwidth and decrease the resistivity, as shown in Fig. 1b and Supplementary Fig. 3. However, in the low-temperature regime ~30 K, the resistivity initially decreases with pressure, followed by a slight increase above 15 kbar (see Fig. 1b and Supplementary Fig. 2). These findings suggest that the high-T_c high-pressure phase harbours additional scattering mechanisms that slightly enhance resistivity and broaden the superconducting-to-normal transition.

The evolution of the Fermi surface with pressure

Figure 2a illustrates the longitudinal magnetoresistance up to 45 T for sample S3 at 0.4 K for pressures up to 22 kbar. The high quality of the crystals and the relatively low upper critical fields allow for the observation of quantum oscillations arising from Landau quantization, which are superimposed on the magnetoresistance background. The frequencies of quantum oscillations, determined by the Onsager relation $F_k = \frac{\hbar}{2\pi e} A_k$, directly correspond to the extremal cross-sectional areas, A_k, of a Fermi surface[30]. At ambient pressure, the magnetotransport data is primarily characterized by a low-frequency oscillation, which has been previously linked to a potential Lifshitz transition at the boundary of the nematic phase[7]. As the pressure increases, the low frequency disappears and the spectrum is dominated by high-frequency oscillations. These frequencies, visible in the raw data (see Fig. 2a, b), are attributed to larger Fermi surface sheets, resembling those found in the tetragonal $FeSe_{1-x}S_x$ system tuned by chemical pressure[7].

Figures 2b and c show the extracted oscillatory signal and the fast Fourier transform spectra which correspond to the cross-sectional areas of the minimum and maximum orbits on different Fermi surface sheets. With increasing pressure, all the frequencies increase in size linearly, surpassing the expected enlargement of the Brillouin zone size (see Supplementary Fig. 14), as seen in Fig. 3d. At ambient pressure, the Fermi surface of $FeSe_{0.82}S_{0.18}$ is anticipated to contain two electron and two hole pockets, based on ARPES and quantum oscillations studies[11,12]. However, DFT calculations tend to overestimate the size of the Fermi surface, requiring band shifts and renormalization to align with the experimental observations, as detailed in Supplementary Fig. 13. Based on the comparison between the data and different simulations, the frequencies, β and δ, are assigned to the minimum and maximum of the outer hole band orbits, whereas ϵ and γ are associated with the outer electron pocket, as shown in Fig. 2d. In addition, the χ frequency corresponds to the maximal orbit of the 3D inner hole, while the two lowest frequencies, α_1 and α_2 are assigned to the small inner electron pocket[11]. Interestingly, the FFT spectra obtained outside the nematic phase exhibit striking similarities between $FeSe_{0.82}S_{0.18}$ at 4.6 kbar and $FeSe_{0.81}S_{0.19}$ at ambient pressure (see Supplementary Fig. 10)[7], implying a similar evolution of the Fermi surface in the tetragonal phase.

In order to gain insights into the intricate alterations in the Fermi surface topography of $FeSe_{0.82}S_{0.18}$ under pressure, we employ a tight-binding-like decomposition of the Fermi vector in cylindrical coordinates. This approach takes into account the allowed symmetries[31], while ensuring charge compensation, as detailed in Supplementary Fig. 8. Since the interlayer compressibility of FeSe under pressure increases by a factor of 2.5 compared to the in-plane (ab) plane value[32], it implies the presence of soft Se-Se interlayer interactions. This, in turn, influences the interplane distortions of the Fermi surface, which can be quantified by the $k_{10} \sim 2\pi/c$ term (see Supplementary Table 1 and Supplementary Fig. 8d). Through a comparison between experimental data and these simulations, we observe that the Fermi surface pockets expand, and the outer hole pocket becomes increasingly two-dimensional as pressure increases. Additionally, the pockets that are most sensitive to interplane distortion are the small inner pockets (see Supplementary Fig. 8c, d). When comparing with the chemical pressure tuning from FeSe to FeS, the hole cylinders increase in size and become less warped compared to the quasi-two-dimensional electron pockets[28]. Thus, both chemical and applied pressure in $FeSe_{1-x}S_x$ mainly result in an expansion of the Fermi surface[7,12,19,28]. However, the enhancement of superconductivity is only achieved through the application of physical pressure.

Quasiparticle effective masses

The damping effects on the quantum oscillations amplitude, caused by temperature and magnetic field, provide direct information about the cyclotron effective mass (see Fig. 2e, f) and scattering times of quasiparticles (Fig. 2h and Supplementary Fig. 11). Figure 2f shows the temperature dependence of the amplitude for each orbit at $p = 11$ kbar (other pressures are in Supplementary Fig. 9), from which the effective masses are extracted using the thermal damping term of the Lifshitz–Kosevich formula[30]. The temperature dependence of the amplitudes of the β and δ hole orbits decrease more rapidly, indicating a larger effective mass (~4 m_e), compared to the χ hole orbit which has a lighter mass (~2 m_e). These results are in good agreement with the values of the inner and outer hole pockets obtained from ARPES studies[11]. The effective masses of the hole pockets show relatively weak variations with applied pressure, despite the significant changes in T_c up to 22 kbar, as shown in Fig. 3f. The effective mass of the χ orbit slightly decreases, while that of the β orbit increases. However, the effective mass associated with the ϵ electron pocket has a higher level of uncertainty due to its weak signal. Overall, the effective masses in $FeSe_{0.82}S_{0.18}$ under pressure are much larger than those detected in FeS, where the largest effective mass is ~2.4 m_e[28]. The effective mass can be enhanced by both electron–electron correlations and electron–phonon coupling as $m^* = m_b(1 + \lambda_{\text{el-ph}})(1 + \lambda_{\text{e-e}})$, where m_b is the band mass[30]. The electron–phonon coupling of FeSe is predicted to slightly increase with applied pressure (from a maximum value $\lambda_{\text{el-ph}} = 0.98$ at 0 kbar to 1.159 at 26 kbar)[33] and it could lead to small increase in the effective mass of 0.4–0.7 m_e, falling within the range of values measured for the hole orbits (see Fig. 3f).

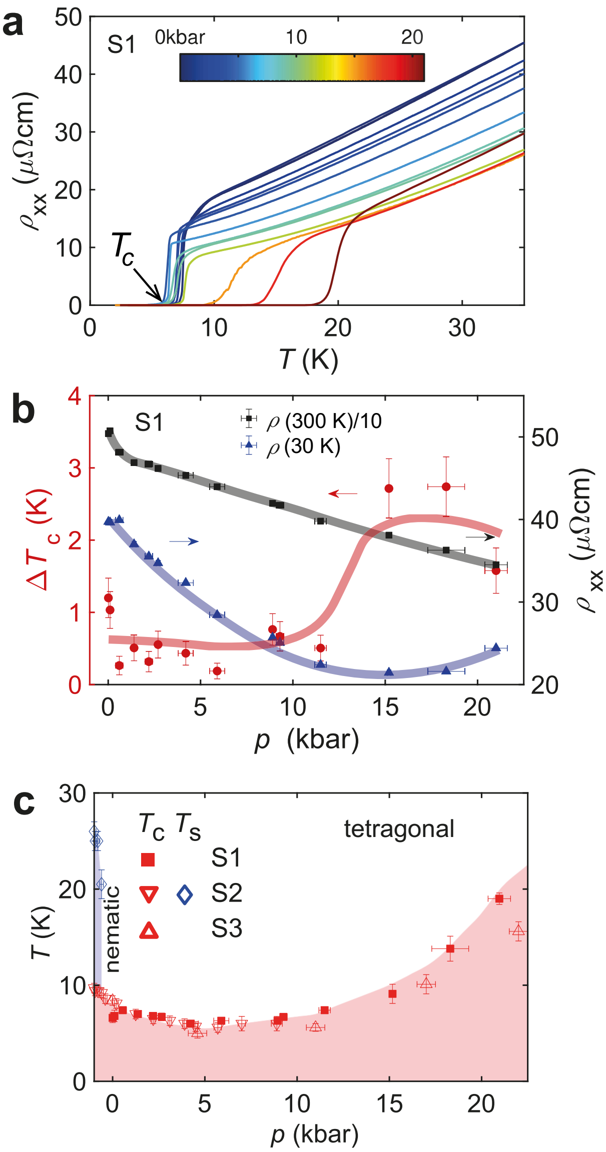

Fig. 1 | Transport behaviour of $FeSe_{0.82}S_{0.18}$ under pressure. **a** The temperature dependence of resistivity for the sample S1 for different applied pressures up to 21 kbar. T_c is defined as the offset superconducting transition temperature (extrapolated towards the zero resistivity state). **b** The superconducting transition width, $\Delta T_c = T_{on} - T_{off}$ (red circles), and resistivity at 300 K (black squares, scaled by a factor of 0.1), and at 30 K (blue triangles) as a function of pressure. Solid lines are guide to the eye. Error bars in transition width are related to the standard deviation of the linear fit tangential to the mid-point transition. **c** The temperature-pressure phase diagram of $FeSe_{0.82}S_{0.18}$ for different single crystals. Sample S1 (solid squares) and S3 (open up triangles) are in the tetragonal phase at ambient pressure. Sample S2 (open down triangles for T_c and open diamonds for the nematic transition, T_s) is just inside the nematic phase corresponding to a negative pressure of −1 kbar, as shown in Supplementary Fig. 1. Error bars in the transition temperatures are estimated from the deviations of the offset temperature from the zero-resistance temperature. Pressure error bars in (**b**, **c**) are related to the width of the tin superconducting transition.

Scattering under pressure

Scattering mechanisms under pressure can be assessed from our measurements at the lowest temperature, as shown in Fig. 2h. The first mechanism is the transport classical scattering time, τ_t, which primarily accounts for large-angle scattering events resulting in significant momentum changes. This can be estimated from the zero temperature resistivity, ρ_0, and considering that the carrier density, n, increases with pressure (Supplementary Fig. 8f). Secondly, the quantum lifetime, τ_q, which encompasses all scattering events, can be extracted from Dingle plots. These reflect the damping of the quantum oscillation amplitude of the δ pocket as a function of the inverse magnetic field at constant temperature (see Supplementary Fig. 11). We find that τ_q varies between 0.5 and 0.7 ps up to 17 kbar (which corresponds to a mean free path close to ~450 Å), similar to values found in the tetragonal phase of $FeSe_{0.89}S_{0.11}$[19] or FeSe[34]. It is worth noting that the values of τ_q is highly sensitive to the background magnetoresistance and any potential interference from the γ pocket at 4.6 kbar, as shown in Supplementary Fig. 11. Moreover, τ_t is larger than τ_q, similar to FeSe[35], and they both increase with applied pressure up to 15 kbar (see Fig. 2h). At the highest pressures ~22 kbar, a significant discrepancy arises between the two scattering times, as the τ_t decreases whereas τ_q increases, as shown in Fig. 2h. Since the original impurity concentration remains constant under pressure, any additional changes in the scattering times indicate modifications in the electronic phase induced at high pressure.

Discussion

The evolution of the electronic structure and effective masses of $FeSe_{0.82}S_{0.18}$ under applied hydrostatic pressure can be compared to the effects of chemical substitution in $FeSe_{1-x}S_x$[7], as illustrated in Fig. 3c, d. The observed frequencies exhibit a linear expansion with increasing pressure, similar to trends observed in the tetragonal phases of $FeSe_{1-x}S_x$[7,19]. This behaviour rules out the reconstruction of the Fermi surface at high pressures, in contrast to FeSe under applied pressure where only a very small pocket was detected[29]. The expansion of the Fermi surface leads to an increase in the carrier density, n, (according to Luttinger's theorem[36]), which doubles in value (Supplementary Fig. 8f). Moreover, the extracted values of the Fermi liquid coefficient, A, decrease with pressure, before flattening off above 15 kbar (see Supplementary Fig. 6), which also reflects the expansion of the Fermi surface. Meanwhile, the value of T_c increases by a factor of 3 over the same pressure range (see Fig. 3g). It is worth noting that FeS has an even larger carrier density, yet its T_c remains relatively small around 5 K[37]. Thus, having a large Fermi surface alone is not sufficient to explain the changes in superconductivity.

The effective masses of the different orbits of the Fermi surface of $FeSe_{0.82}S_{0.18}$ remain almost unchanged under pressure, in particular, the value for the δ orbit is only slightly lighter in the tetragonal phase as compared to the nematic phase[7]. The effective mass for a quasi-two-dimensional system is related to the density of states at the Fermi level, $g(E_F) \sim m^*/(\pi\hbar^2)$. Thus, it is expected that higher T_c in $FeSe_{0.82}S_{0.18}$ could be associated with the larger effective masses, in comparison with FeS, which has lower T_c and lighter masses. These experimental observations are further supported by the estimated density of states based on the adjusted Fermi surfaces based on DFT calculations, as shown in Supplementary Fig. 14f. One parameter which influences density of states is the chalcogen height above the Fe planes, h, (see Supplementary Fig. 14) which increases under applied pressure (~1.45 Å at 18.2 kbar in $FeSe_{0.80}S_{0.20}$[38], but decreases for FeS at ambient pressure (1.269 Å)[29]). However, the observed variation in effective masses of the hole pockets is minimal under applied pressure (see Fig. 3f). Therefore, the significant enhancement of T_c at high pressure requires an additional ingredient to boost the superconducting pairing (see Fig. 3h).

In order to enhance the superconducting transition temperature T_c by a factor of three, either the contribution to $g(E_F)$ from other pockets increases, or an additional pairing interaction becomes operative under pressure (SC2 regime in Fig. 3b). One potential mechanism involves shifting the hole pocket with d_{xy} orbital character close to the Fermi level, as found in $FeSe_{1-x}Te_x$[39]. The presence of a third hole pocket is predicted to enhance the spin fluctuations in the d_{xy} channel increasing the pairing interaction[40]. However, our quantum oscillations do not detect a third hole pocket. Alternatively, the heavy electron pockets, whose orbits ϵ, γ have regions with $d_{xz/yz}$ and d_{xy} orbital character (see Fig. 2c) could become even more correlated under pressure and potentially contribute to the missing density of states. Interestingly, systems containing only electron pockets, like electron-doped intercalated FeSe systems[41] or the FeSe monolayer grown on $SrTiO_3$ have a higher T_c exceeding 40 K. Thus, pairing channels involving electron pockets could be potentially enhanced under high pressures[8,42].

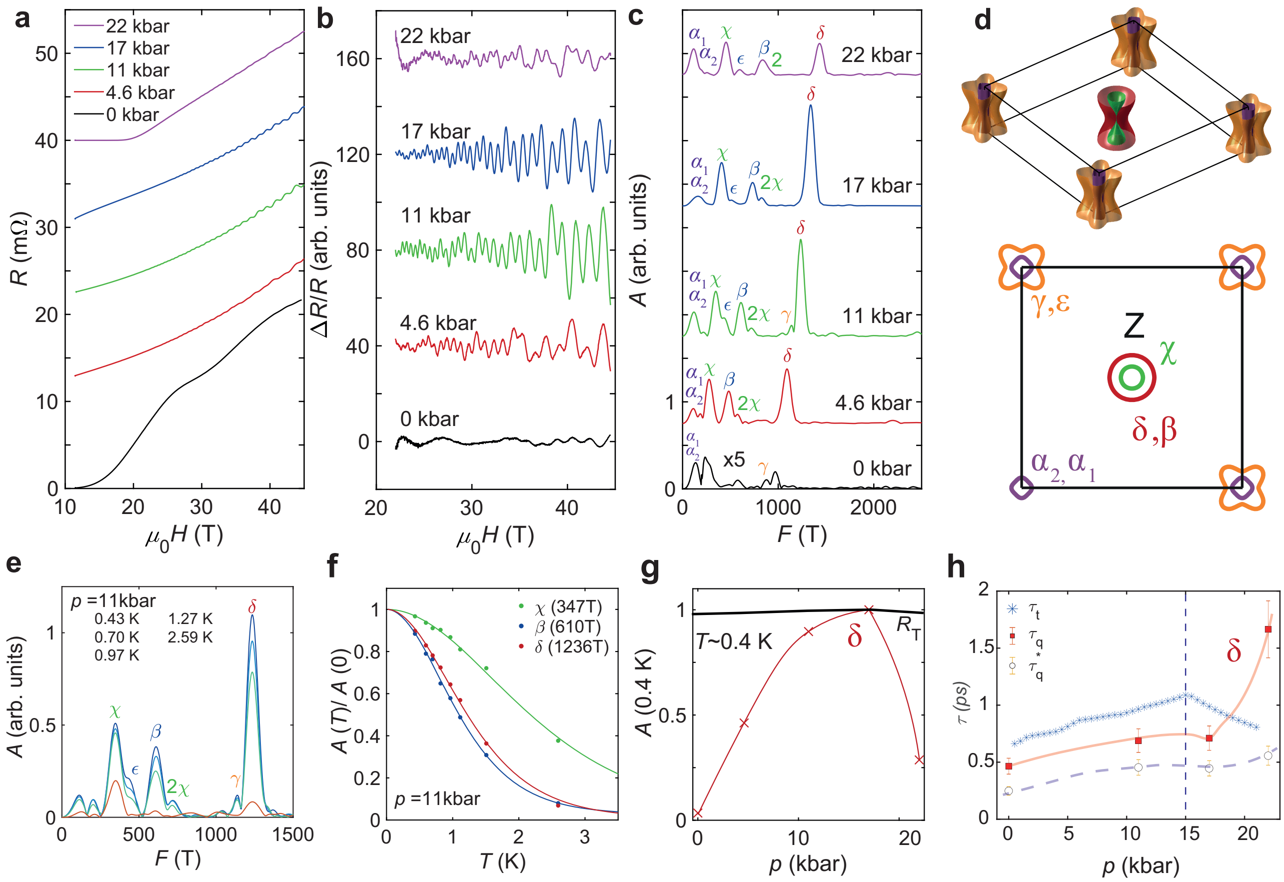

Fig. 2 | Evolution of quantum oscillations with pressure in $FeSe_{0.82}S_{0.18}$. **a** Longitudinal resistivity measurements in magnetic fields up to 45 T at 0.4 K for a range of pressures. **b** Shubnikov-de Haas oscillations obtained from extracting the background magnetoresistance described by a seven-order polynomial over a window $\mu_0\Delta H = 22 - 45$ T. **c** Fast Fourier transforms (FFT) of the signal in (**b**) using a Hanning windowing function having the different peaks and the corresponding harmonics labelled. The ambient signal is amplified five times above 200 T and curves in panels (**a**–**c**) are shifted vertically for clarity. **d** The proposed quasi-3D Fermi surface of $FeSe_{0.82}S_{0.18}$ and the slice at the top of the Brillouin zone, $k_z = \pi/c$. **e** FFT amplitude spectra at different temperatures for $p = 11$ kbar. Amplitude is fitted to the Lifshitz–Kosevich formula[30] to determine the quasiparticle effective masses of each orbit in (**f**). **g** The pressure dependence of the FFT amplitudes of the main peaks at base temperature of ~0.4 K. The solid line corresponds to the values of R_T term normalized at the 17 kbar value. **h** The changes in the quantum, τ_q and classical scattering time, τ_t, as a function of pressure. τ_q is estimated from Dingle plots at ~ 0.4K by filtering the δ orbit and τ_q^* is obtained from the subtracted signal ΔR and error bars are standard deviations in linear fits (see Supplementary Fig. S11). The classical time is estimated from the resistivity data in Supplementary Fig. 2. The solid and dashed lines are guides to the eye and the vertical dashed line indicates the position at which the classical time reaches its largest value.

The increase in the density of states at the Fermi level, $g(E_F)$ under pressure, can contribute to the stabilization of magnetically ordered states based on the Stoner criteria ($I \cdot g(E_F) > 1$, where I is the Stoner coefficient). The density of states can be enhanced with increasing chalcogen height, under applied pressure[43], or by the isoelectronic substitution with Te[44], which create conditions to stabilize magnetically ordered phases. The nearest-neighbour Coulomb repulsion and electronic correlations in FeSe would generally decrease with pressure and lead to enhanced spin fluctuations[45]. The nesting between large and isotropic pockets with large Fermi energy (50 meV at 22 kbar as shown in Fig. 3g) in the presence of a larger density of states could induce a spin-density wave[5]. While in our system, the density of states increases under pressure, we do not detect any clear anomalies in resistivity associated to a spin-density wave up to 22 kbar, which was proposed to occur around 50 kbar[18]. On the other hand, FeSe shows a magnetic phase under pressure and quantum oscillations only detect a very small pocket with light effective mass, potentially reflecting the Fermi surface reconstruction[29]. Unusually, NMR studies in $FeSe_{1-x}S_x$ find weak and potentially short-range spin fluctuations in the tetragonal phase at high pressures[46], different from strong stripe-type AFM spin fluctuations were found inside the nematic phase[47].

The high-pressure high-T_c phase exhibits distinct electronic signatures compared to the nematic phase of $FeSe_{1-x}S_x$ systems. Firstly, there is no correlation between the strong enhancement of T_c and the effective mass of the δ hole orbit (Fig. 3b, f), contrary to the trends observed inside the nematic phase (see Fig. 3a, e)[12,14,19]. Secondly, there are significant differences in spin fluctuations which are mainly detected only inside the nematic phase[47], but could transform into short-range correlations in the tetragonal phase at high pressures[46,48]. Thirdly, there is a notable difference between the quantum and classical scattering times, and the amplitude of the δ hole orbit is significantly suppressed (see Fig. 2a, g and Supplementary Fig. 4). Lastly, the superconducting transition broadens both in temperature and field, accompanied by a reduction in the oscillatory signal relative to the background magnetoresistance (see Supplementary Fig. 5).

Interestingly, superconductivity is enhanced under pressure for various $FeSe_{1-x}S_x$ systems, even in the presence of Cu impurities[23]. Thus, the high-T_c phase in $FeSe_{1-x}S_x$ demonstrates remarkable robustness to impurities and substitutions, indicating a potential non-sign changing pairing mechanism and reduced sensitivity to any long-range magnetic order. At very high pressures (50 kbar) in $FeSe_{0.89}S_{0.11}$ both the superconductivity and metallicity are lost[24], and the diamagnetic signal is suppressed[49], triggered by the development of uniaxial pressure effects. These effects may reflect a complex high-pressure phase having different conductivity channels at high pressures[50], or be dominated by strong magnetic or superconducting fluctuations[43,51]. Alternatively, the distribution of chalcogen ions outside the

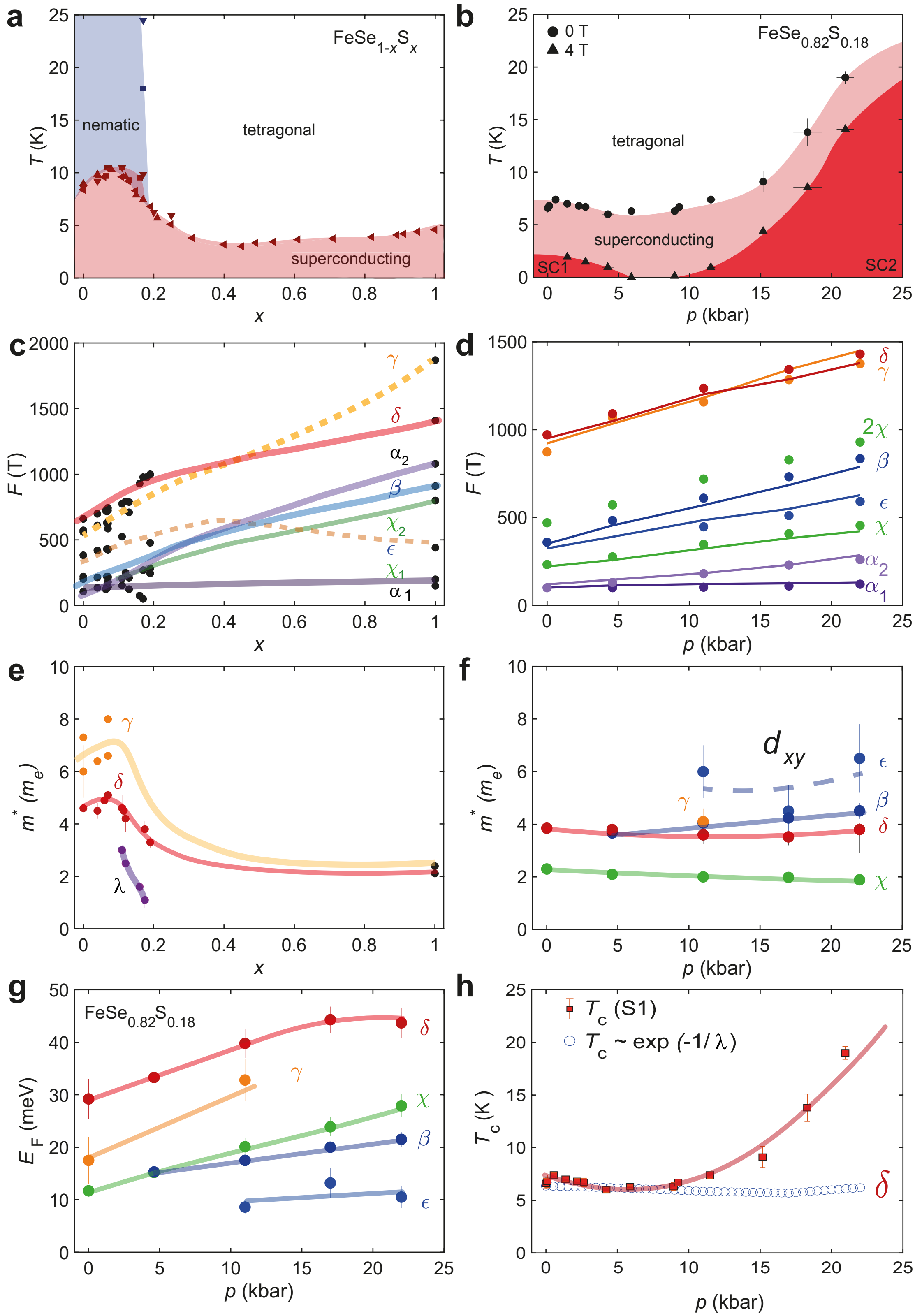

Fig. 3 | Comparison between the physical and chemical pressure effects. a The phase diagram of $FeSe_{1-x}S_x$ tuned by the sulphur substitution x (after ref. 7) and **b** the $p-T$ phase diagram of $FeSe_{0.82}S_{0.18}$ up to 22 kbar, in 0 T (as in Fig. 1g) and in 4 T field (darker areas), which separates two regimes of superconductivity (SC1 and SC2). Error bars are related to the superconducting transition width. Frequencies extracted from quantum oscillations for (**c**) $FeSe_{1-x}S_x$ versus x (after refs. 7 and [28]) and **d** $FeSe_{0.82}S_{0.18}$ versus pressure. Error bars for the frequency are related the the half maximum of the FFT widths, and error bars for the effective mass are standard deviations from LK fitting. The corresponding quasiparticle effective masses, m^*, are in (**e**, **f**), respectively. Solid and dashed lines are guide to the eye. **g** The calculated Fermi energy, E_F for $FeSe_{0.82}S_{0.18}$ assuming parabolic band dispersion using the values in (**d**, **f**). Error bars are propagated from errors of frequencies and effective masses. **h** The pressure dependence of the T_c for S1 (solid square) and a rough estimate assuming a BCS dependence which depends only on the density of states of a quasi-2D pocket for the δ pocket (open circles). Error bars are related to the superconducting transition width.

conducting planes could create conditions to develop electronic inhomogeneities and quantum Griffiths phases[52] or potential short-range stripe patterns of incipient charge order correlations[53].

The electron–phonon coupling could also play a role in stabilizing higher superconducting phase in the high pressure in $FeSe_{1-x}S_x$, similar to other high-T_c iron-based superconductors. Raman studies in the electron-doped intercalated (Li,Fe)OHFeSe suggest that lattice-induced orbital fluctuations are responsible for pairing[41], whereas in the monolayer FeSe on interfacial coupling with the oxygen optical phonons in SrTiO3 could play an important role[42]. The lattice itself is sensitive to pressure-induced changes, and the chalcogen height influences the out-of-plane phonon mode, A_{1g} and the electron–phonon coupling[33]. In such cases, local deformation potentials can result in strong coupling between electrons and the lattice, forming polarons[33] which could condense as pairs in bipolarons[54]. In the presence of electronic correlations, the electron–phonon coupling could be further enhanced in FeSe[55,56]. Thus, the route to induce a high-T_c phase under applied pressure phase could be promoted by the formation of an electronic phase, with different quasiparticles, in which lattice effects can influence the density of states, the strength of electronic correlations and it can lead to unconventional scattering.

Methods

Single-crystal characterization

Single crystals of $FeSe_{0.82}S_{0.18}$ were grown by the KCl/$AlCl_3$ chemical vapour transport method, as reported previously[10,57]. More than 10 crystals were screened at ambient pressure and were found to have large residual resistivity ratios (*RRR*) up to 25 between room temperature and the onset of superconductivity. Crystals from the same batch were previously used in quantum oscillations and ARPES studies[7,11]. All samples measured were from the same batch and EDX measurements measured the composition to contain a sulphur content of $x = 0.18(1)$, which places the batch in the vicinity of the nematic end point[11,12].

High-pressure studies in magnetic fields

High magnetic field measurements up to 45 T at ambient pressure and under hydrostatic pressure were performed using the hybrid magnet dc facility at the NHMFL in Tallahassee, FL, USA on sample S3. Pressures up to 22 kbar were generated using a MP35N piston-cylinder cell, using Daphne Oil 7575 as pressure medium. The pressure inside the cell was determined by means of ruby fluorescence at low temperatures where quantum oscillations were observed. Magnetotransport and Hall effect measurements under pressure using a 5-contact configuration were carried out on samples S1 and S2 in low fields up to 16 T in Oxford using the Quantum Design PPMS and an ElectroLab High-Pressure Cell, using Daphne Oil 7373 which ensures hydrostatic conditions up to about 21 kbar. The pressure inside this cell was determined via the superconducting transition temperature of Sn after cancelling the remnant field in the magnet. The magnetic field was applied along the crystallographic *c* axis for all samples. A maximum current of up to 2 mA flowing in the conducting tetragonal *ab* plane was used. The cooling rate was kept 0.5 K/min below 100 K to reduce the thermal lag between the sample and the pressure cell.

Quantum oscillations

The amplitude of the quantum oscillations is affected by different damping terms given by the Lifshitz–Kosevich equation[30]. The thermal damping term, $R_T = \frac{X}{\sinh}(X)$, where $X = \frac{2\pi^2 k_B T p m^*}{e\hbar B}$, enables to extract the quasiparticle effective masses m^*, and the Dingle term, $R_D = \exp\left(-\frac{\pi p m^*}{e B \tau_q}\right)$, allows to estimate the quantum scattering rate τ_q (or the mean free path ℓ using the equivalent expression $R_D = \exp\left(-1140\frac{\sqrt{F}}{\ell B}\right)$[58]. Other damping factors which have exponential forms could be caused by small random sample inhomogeneities, magnetic field inhomogeneities and additional damping within the vortex regime[59].

Data availability

All data are available in the manuscript or the supplementary materials. The data that support the findings of this study will be available through the open-access data archive at the University of Oxford (ORA) at https://doi.org/10.5287/ora-9ryyqkw8v. Additional information about the data will be made available from the corresponding author upon reasonable request.

Received: 7 September 2023; Accepted: 27 June 2024;

References

1. Drozdov, A. P. et al. Superconductivity at 250 K in lanthanum hydride under high pressures. *Nature* **569**, 528–531 (2019).
2. Medvedev, S. et al. Electronic and magnetic phase diagram of β-$Fe_{1.01}Se$ with superconductivity at 36.7 K under pressure. *Nat. Mater.* **8**, 630 (2009).
3. Kothapalli, K. et al. Strong cooperative coupling of pressure-induced magnetic order and nematicity in FeSe. *Nat. Comm.* **7**, 12728 (2016).
4. Sun, J. P. et al. Dome-shaped magnetic order competing with high-temperature superconductivity at high pressures in FeSe. *Nat. Commun.* **7**, 12146 (2016).
5. Chubukov, A. V., Khodas, M. & Fernandes, R. M. Magnetism, superconductivity, and spontaneous orbital order in iron-based superconductors: which comes first and why? *Phys. Rev. X* **6**, 041045 (2016).
6. Sprau, P. O. et al. Discovery of orbital-selective cooper pairing in FeSe. *Science* **357**, 75 (2016).
7. Coldea, A. I. et al. Evolution of the low-temperature Fermi surface of superconducting $FeSe_{1-x}S_x$ across a nematic phase transition. *NPJ Quantum Mater.* **4**, 2 (2019).
8. Kreisel, A., Hirschfeld, P. J. & Andersen, B. M. On the remarkable superconductivity of FeSe and its close cousins. *Symmetry* **12**, 1402 (2020).
9. Bendele, M. et al. Coexistence of superconductivity and magnetism in $FeSe_{1-x}$ under pressure. *Phys. Rev. B* **85**, 064517 (2012).
10. Böhmer, A. E., Taufour, V., Straszheim, W. E., Wolf, T. & Canfield, P. C. Variation of transition temperatures and residual resistivity ratio in vapor-grown FeSe. *Phys. Rev. B* **94**, 024526 (2016).
11. Reiss, P. et al. Suppression of electronic correlations by chemical pressure from FeSe to FeS. *Phys. Rev. B* **96**, 121103 (2017).
12. Coldea, A. I. Electronic nematic states tuned by isoelectronic substitution in bulk $FeSe_{1-x}S_x$. *Front. Phys.* **8**, 528 (2021).
13. Hosoi, S. et al. Nematic quantum critical point without magnetism in $FeSe_{1-x}S_x$ superconductors. *Proc. Natl. Acad. Sci. USA* **113**, 8139 (2016).
14. Bristow, M. et al. Anomalous high-magnetic field electronic state of the nematic superconductors $FeSe_{1-x}S_x$. *Phys. Rev. Res.* **2**, 013309 (2020).
15. Hanaguri, T. et al. Two distinct superconducting pairing states divided by the nematic end point in $FeSe_{1-x}S_x$. *Sci. Adv.* **4**, eaar6419 (2018).
16. Sato, Y. et al. Abrupt change of the superconducting gap structure at the nematic critical point in $FeSe_{1-x}S_x$. *Proc. Natl. Acad. Sci. USA* **115**, 1227–1231 (2018).
17. Setty, C., Bhattacharyya, S., Cao, Y., Kreisel, A. & Hirschfeld, P. J. Topological ultranodal pair states in iron-based superconductors. *Nat. Commun.* **11**, 523 (2020).
18. Matsuura, K. et al. Maximizing T_c by tuning nematicity and magnetism in $FeSe_{1-x}S_x$ superconductors. *Nat. Comm.* **8**, 1143 (2017).
19. Reiss, P. et al. Quenched nematic criticality and two superconducting domes in an iron-based superconductor. *Nat. Phys.* **16**, 89–94 (2020).
20. Rana, K. et al. Impact of nematicity on the relationship between antiferromagnetic fluctuations and superconductivity in $FeSe_{0.91}S_{0.09}$ under pressure. *Phys. Rev. B* **101**, 180503 (2020).
21. Xiang, L. et al. Dome of magnetic order inside the nematic phase of sulfur-substituted FeSe under pressure. *Phys. Rev. B* **96**, 024511 (2017).

22. Xie, J. et al. Fragile pressure-induced magnetism in FeSe superconductors with a thickness reduction. *Nano Lett.* **21**, 9310–9317 (2021).
23. Zajicek, Z., Singh, S. J. & Coldea, A. I. Robust superconductivity and fragile magnetism induced by the strong Cu impurity scattering in the high-pressure phase of FeSe. *Phys. Rev. Res.* **4**, 043123 (2022).
24. Reiss, P., McCollam, A., Zajicek, Z., Haghighirad, A. A. & Coldea, A. I. Collapse of metallicity and high-T_c superconductivity in the high-pressure phase of $FeSe_{0.89}S_{0.11}$. Preprint at https://arxiv.org/abs/2212.06824 (2022).
25. Terashima, T. et al. Anomalous Fermi surface in FeSe seen by Shubnikov-de Haas oscillation measurements. *Phys. Rev. B* **90**, 144517 (2014).
26. Watson, M. D. et al. Emergence of the nematic electronic state in FeSe. *Phys. Rev. B* **91**, 155106 (2015).
27. Audouard, A. et al. Quantum oscillations and upper critical magnetic field of the iron-based superconductor FeSe. *Europhys. Lett.* **109**, 27003 (2015).
28. Terashima, T. et al. Accurate determination of the Fermi surface of tetragonal FeS via quantum oscillation measurements and quasiparticle self-consistent GW calculations. *Phys. Rev. B* **99**, 134501 (2019).
29. Terashima, T. et al. Fermi surface reconstruction in FeSe under high pressure. *Phys. Rev. B* **93**, 094505 (2016).
30. Shoenberg, D. *Magnetic Oscillations in Metals* (Cambridge University Press, 1984).
31. Bergemann, C., Julian, S. R., Mackenzie, A. P., NishiZaki, S. & Maeno, Y. Detailed topography of the Fermi Surface of Sr_2RuO_4. *Phys. Rev. Lett.* **84**, 2662–2665 (2000).
32. Margadonna, S. et al. Pressure evolution of the low-temperature crystal structure and bonding of the superconductor FeSe (T_c = 37K). *Phys. Rev. B* **80**, 064506 (2009).
33. Mandal, S., Cohen, R. E. & Haule, K. Strong pressure-dependent electron-phonon coupling in FeSe. *Phys. Rev. B* **89**, 220502 (2014).
34. Watson, M. D. et al. Dichotomy between the hole and electron behavior in multiband superconductor FeSe probed by ultrahigh magnetic fields. *Phys. Rev. Lett.* **115**, 027006 (2015).
35. Farrar, L. S. et al. Unconventional localization of electrons inside of a nematic electronic phase. *Proc. Natl. Acad. Sci. USA* **119**, e2200405119 (2022).
36. Luttinger, J. M. & Ward, J. C. Ground-state energy of a many-fermion system. ii. *Phys. Rev.* **118**, 1417–1427 (1960).
37. Terashima, T. et al. Upper critical field and quantum oscillations in tetragonal superconducting FeS. *Phys. Rev. B* **94**, 100503 (2016).
38. Tomita, T. et al. Correlation between T_c and crystal structure in S-doped FeSe superconductors under pressure: studied by X-ray diffraction of $FeSe_{0.8}S_{0.2}$ at low temperatures. *J. Phys. Soc. Jpn.* **84**, 024713 (2015).
39. Morfoot, A. B. et al. Resurgence of superconductivity and the role of d_{xy} hole band in $FeSe_{1-x}Te_x$. *Commun. Phys.* **6**, 362 (2023).
40. Yamakawa, Y. & Kontani, H. Nematicity, magnetism, and superconductivity in FeSe under pressure: unified explanation based on the self-consistent vertex correction theory. *Phys. Rev. B* **96**, 144509 (2017).
41. Xiao, Q. et al. Dispersionless orbital excitations in (Li,Fe)OHFeSe superconductors. *NPJ Quantum Mater.* **7**, 80 (2022).
42. Lee, D.-H. Routes to high-temperature superconductivity: a lesson from FeSe/$SrTiO_3$. *Annu. Rev. Condens. Matter Phys.* **9**, 261–282 (2018).
43. Okabe, H., Takeshita, N., Horigane, K., Muranaka, T. & Akimitsu, J. Pressure-induced high-T_c superconducting phase in FeSe: correlation between anion height and T_c. *Phys. Rev. B* **81**, 205119 (2010).
44. Kumar, J., Auluck, S., Ahluwalia, P. K. & Awana, V. P. S. Chalcogen height dependence of magnetism and fermiology in $FeTe_xSe_{1-x}$. *Superconductor Sci. Technol.* **25**, 095002 (2012).
45. Scherer, D. D. et al. Interplay of nematic and magnetic orders in FeSe under pressure. *Phys. Rev. B* **95**, 094504 (2017).
46. Rana, K. et al. Interrelationships between nematicity, antiferromagnetic spin fluctuations, and superconductivity: Role of hotspots in $FeSe_{1-x}S_x$ revealed by high pressure ^{77}Se NMR study. *Phys. Rev. B* **107**, 134507 (2023).
47. Wiecki, P. et al. Persistent correlation between superconductivity and antiferromagnetic fluctuations near a nematic quantum critical point in $FeSe_{1-x}S_x$. *Phys. Rev. B* **98**, 020507 (2018).
48. Kuwayama, T. et al. Pressure-induced reconstitution of Fermi surfaces and spin fluctuations in S-substituted FeSe. *Sci. Rep.* **11**, 17265 (2021).
49. Yip, K. Y. et al. Weakening of the diamagnetic shielding in $FeSe_{1-x}S_x$ at high pressures. *Phys. Rev. B* **96**, 020502 (2017).
50. Ayres, J. et al. Transport evidence for decoupled nematic and magnetic criticality in iron chalcogenides. *Commun. Phys.* **5**, 100 (2022).
51. Gati, E., Böhmer, A. E., Bud'ko, S. L. & Canfield, P. C. Bulk superconductivity and role of fluctuations in the iron-based superconductor FeSe at high pressures. *Phys. Rev. Lett.* **123**, 167002 (2019).
52. Reiss, P., Graf, D., Haghighirad, A. A., Vojta, T. & Coldea, A. I. Signatures of a quantum griffiths phase close to an electronic nematic quantum phase transition. *Phys. Rev. Lett.* **127**, 246402 (2021).
53. Walker, M. et al. Electronic stripe patterns near the Fermi level of tetragonal Fe(Se,S). *NPJ Quantum Mater.* **8**, 60 (2023).
54. Zhao, G.-M., Hunt, M. B., Keller, H. & Müller, K. A. Evidence for polaronic supercarriers in the copper oxide superconductors $La_{2-x}Sr_xCuO_4$. *Nature* **385**, 236–239 (1997).
55. Gerber, S. et al. Femtosecond electron-phonon lock-in by photoemission and X-ray free-electron laser. *Science* **357**, 71–75 (2017).
56. Ding, W. et al. Correlation-enhanced electron-phonon coupling for accurate evaluation of the superconducting transition temperature in bulk FeSe. *Sci. China Phys. Mech. Astron.* **65**, 267412 (2022).
57. Böhmer, A. E. et al. Lack of coupling between superconductivity and orthorhombic distortion in stoichiometric single-crystalline FeSe. *Phys. Rev. B* **87**, 180505 (2013).
58. Carrington, A. Quantum oscillation studies of the Fermi surface of iron-pnictide superconductors. *Rep. Prog. Phys.* **74**, 124507 (2011).
59. Rourke, P. M. C. et al. A detailed de Haas-van Alphen effect study of the overdoped cuprate $Tl_2Ba_2CuO_{6+\delta}$. *N. J. Phys.* **12**, 105009 (2010).

Acknowledgements

The authors thank Roemer Hinlopen for the development of the software to model the Fermi surface, and Matthew Bristow for computational support. The authors thank Steve Simon and Sean Hartnoll for useful discussions. This work was mainly supported by EPSRC (EP/I004475/1, EP/I017836/1). A.A.H. acknowledges the financial support of the Oxford Quantum Materials Platform Grant (EP/M020517/1). The research was partly funded by the Oxford Centre for Applied Superconductivity at Oxford University. We also acknowledge financial support from the John Fell Fund of Oxford University. A portion of this work was performed at the National High Magnetic Field Laboratory, which is supported by National Science Foundation Cooperative Agreement No. DMR-1157490 and the State of Florida. Z.Z. acknowledges financial support from EPSRC Studentships EP/N509711/1 and EP/R513295/1. J.C.A.P. acknowledges the support of St. Edmund Hall, University of Oxford, through the Cooksey Early Career Teaching and Research Fellowship. The DFT calculations were performed on the University of Oxford Advanced Research Computing Service. AIC is grateful to KITP for hospitality and this research was supported in part by the National Science Foundation under Grants No. NSF PHY-1748958 and PHY-

2309135. A.I.C. acknowledges EPSRC Career Acceleration Fellowship EP/I004475/1.

Author contributions

P.R., Z.Z., D.G. and A.I.C. performed transport experiments under pressure. Z.Z., P.R. and A.I.C. analysed the transport and quantum oscillation data. A.A.H. synthesized single crystals. J.C.A.P. performed DFT calculations. Y.S. performed the Dingle analysis. A.I.C. and Z.Z. wrote the paper with inputs from all authors. A.I.C. supervised the projects.

Competing interests

The authors declare no competing interests.

Additional information

Supplementary information The online version contains supplementary material available at https://doi.org/10.1038/s41535-024-00663-1.

Correspondence and requests for materials should be addressed to A. I. Coldea.